Accurate Graphene-Metal Junction Characterization

**MATTHIAS KÖNIG[1,2], GÜNTHER RUHL[2], AMIT GAHOI[1], SEBASTIAN WITTMANN[2], TOBIAS PREIS[3],
JOERG-MARTIN BATKE[2], IOAN COSTINA[4], AND MAX C. LEMME** [1,5] **(Senior Member, IEEE)**

1 Faculty of Electrical Engineering and Information Technology, Chair of Electronic Devices, RWTH Aachen University, 52074 Aachen, Germany
2 Frontend Technologies, Infineon Technologies AG, 93049 Regensburg, Germany
3 Institut für Experimentelle und Angewandte Physik, University Regensburg, 93040 Regensburg, Germany
4 Technology Department, IHP, 15236 Frankfurt (Oder), Germany
5 Advanced Microelectronic Center Aachen, AMO GmbH, 52074 Aachen, Germany

CORRESPONDING AUTHOR: M. C. LEMME (e-mail: lemme@amo.de)

ABSTRACT A reliable method is proposed for measuring specific contact resistivity (ρ_C) for graphene-metal contacts, which is based on a contact end resistance measurement. We investigate the proposed method with simulations and confirm that the sheet resistance under the metal contact (R_{SK}) plays an important role, as it influences the potential barrier at the graphene-metal junction. Two different complementary metal-oxide-semiconductor—compatible aluminum-based contacts are investigated to demonstrate the importance of the sheet resistance under the metal contact: the difference in R_{SK} arises from the formation of insulating aluminum oxide (Al_2O_3) and aluminum carbide (Al_4C_3) interfacial layers, which depends on the graphene pretreatment and process conditions. Auger electron spectroscopy and X-ray photoelectron spectroscopy support electrical data. The method allows direct measurements of contact parameters with one contact pair and enables small test structures. It is further more reliable than the conventional transfer length method when the sheet resistance of the material under the contact is large. The proposed method is thus ideal for geometrically small contacts where it minimizes measurement errors and it can be applied in particular to study emerging devices and materials.

INDEX TERMS Graphene, electrical contacts, TLM.

I. INTRODUCTION

Low specific contact resistivity (ρ_C) is one of the crucial parameters for the integration of graphene into nanoelectronic devices. Typical critical device dimensions are in the range of 10 to 100 nm, so it is imperative that ρ_C is extremely small to fabricate high performance graphene-based devices. The specific contact resistivity is derived from the graphene-metal interfacial resistance, whereas the contact resistance is a combination of graphene sheet resistance and specific contact resistance. The specific contact resistivity (ρ_C) of typical metal silicides/silicon contacts are in the range of 10^{-7} - $10^{-8}\Omega cm^2$ [1]–[3]. However, unstable process conditions may lead to the formation of interface oxides that increase ρ_C to the range of 10^{-5} - $10^{-6}\Omega cm^2$ [4], [5]. In graphene-metal junctions, in contrast, current tends to flow primarily through the edge of the contact, i.e., the least resistance path [6]. This is mainly the case for geometrically large contacts, as in widely used test structures, because the area of the contact can be neglected. For real world applications, contacts need to be much smaller and lower levels of ρ_C are required. The proposed method, based on TLM and contact end resistance methods, is able to measure both ρ_C and R_C, which enables contact investigations in a more general way, as R_C depends on the length of the contact.

Graphene technology is less mature and, as a consequence, R_C has been found to vary widely at graphene-metal junctions from $k\Omega\mu m$ down to several tens of $\Omega\mu m$ [7]–[11]. The major intrinsic factor that results in high ρ_C is the low density of states (DOS) available in graphene under the metal contact [12]. As a consequence, ρ_C, depends on the Fermi
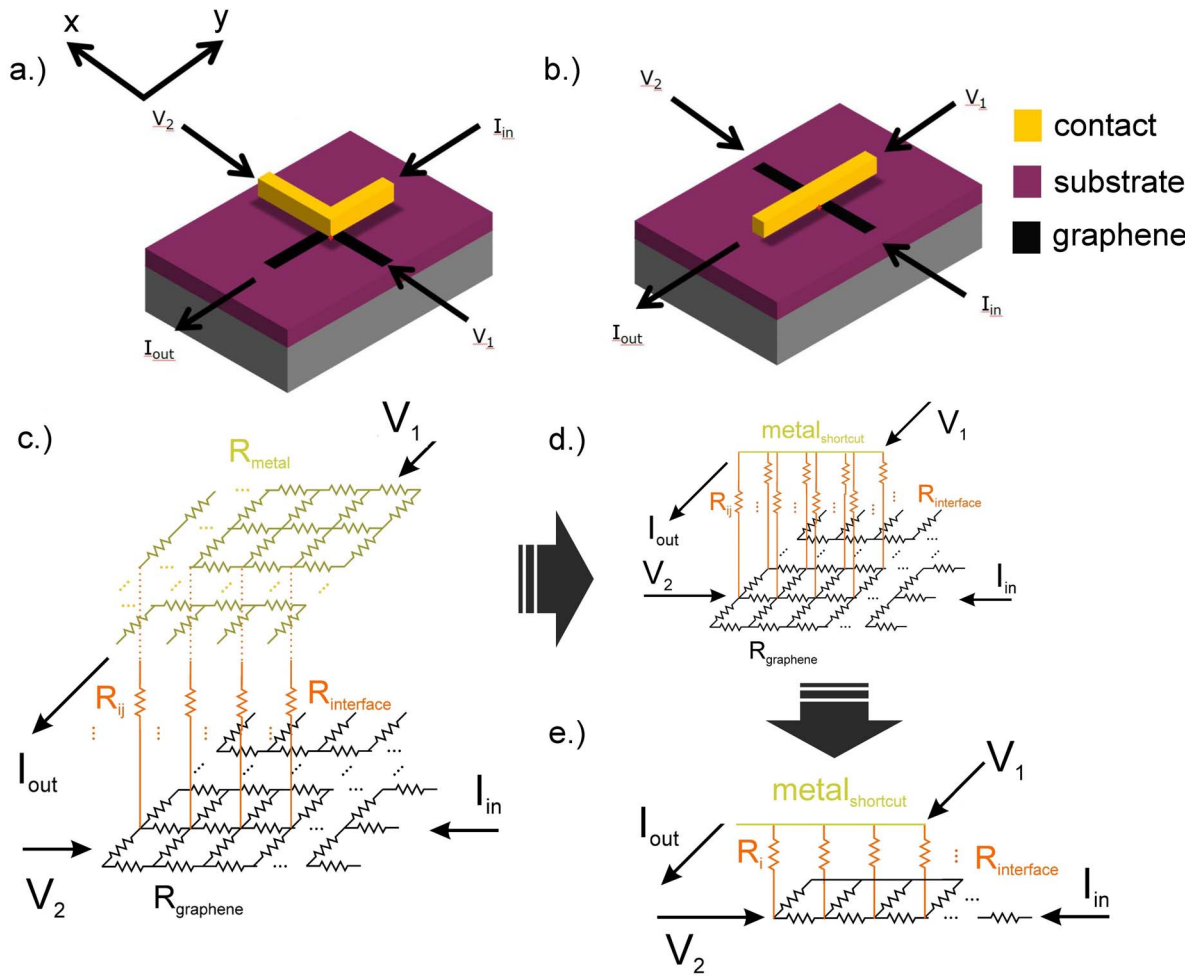
FIGURE 1. (a) Schematic of the standard four terminal method for the extraction of contact resistance. (b) Schematic of contact end resistance method. If the metal resistance can be neglected, the structure will yield the same result as in (a). This is a valid assumption in the case of graphene-metal contacts. The origin in both images is marked with a red dot. (c) Schematic of the distributed resistor network describing the situation in (b). d) Schematic of the resistor network in (c) when neglecting the metal resistance. The network becomes symmetric, resulting in an equivalent circuit diagram (e). Equivalent circuit diagram like in (d): For symmetry reasons the resistors in the x-direction can be combined compared to (d).

level of the graphene under the metal contact [12], [13]. Another factor is the transport in the graphene under the metal [14]. Finally, process and material aspects can influence ρ_C if carbides or oxides form at the graphene-metal junction [14], [15]. In the latter case, extracting ρ_C by the conventional transfer length method (TLM) or the Cross-Bridge Kelvin Resistor (CBKR) method is prone to errors. Therefore, we propose a technique for the direct measurement of ρ_C and the sheet resistance under the contact (R_{SK}) for graphene-metal junctions on a single contact pair. This has the advantage of a direct and fair comparison of R_{SK} and ρ_C, and can be fabricated with a self-aligned process [15]. We demonstrate the technique with two specific examples and utilize Auger electron spectroscopy (AES) and X-Ray Photoelectron Spectroscopy (XPS) measurements to characterize the materials at the contact area.

II. TEST STRUCTURE AND SIMULATIONS

A simple model to investigate contacts is the "ρ_C - R_{SH} equivalent circuit" [16]. R_{SH} is the sheet resistance of the graphene outside the contact, i.e., without any interaction with the contact material. When current flows from metal to graphene or vice versa it encounters the resistances via ρ_C and R_{SH}, which can be explained by the transmission line model, assuming one-dimensional current flow to the contact interface. A typical electrical contact in semiconductor industry is not defined as a two-dimensional contact between two materials. Instead, it is a three dimensional structure that is typically described as via in a dielectric layer. Nevertheless, the main physics and chemistry at the interface can be studied and optimized without dielectrics and vias, as is the case in this study. Hence we do not expect a different outcome when using a via. At the graphene-metal junction, the potential drop consists of three components

(a) Potential drop due to R_M (metal sheet resistance), which is generally neglected.

(b) Potential drop due to graphene-metal interfacial resistance, i.e., a vertical component.

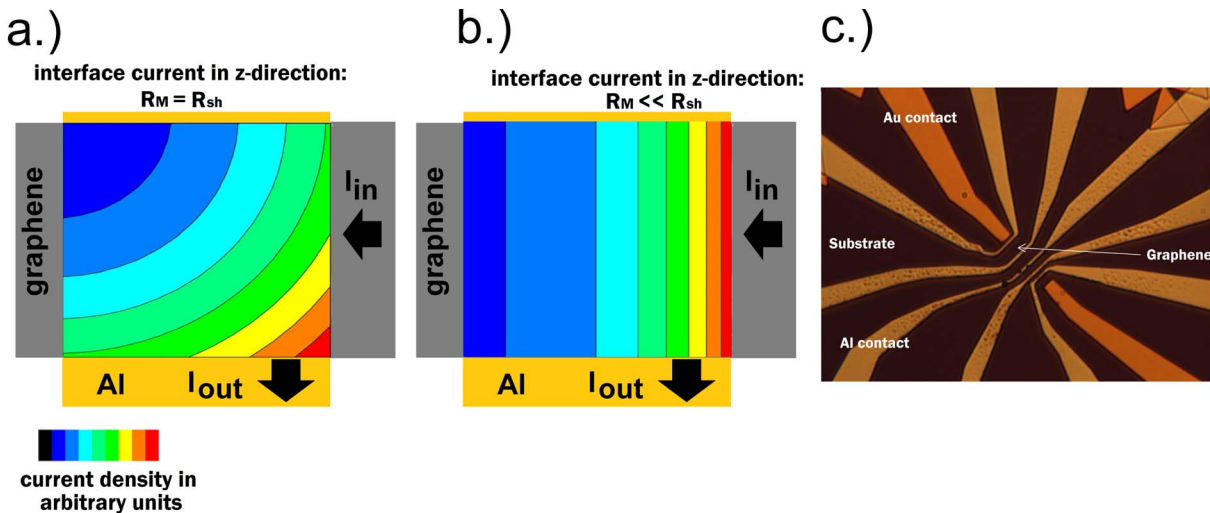(c) Potential drop due to the channel resistance, i.e., a horizontal graphene component.

FIGURE 2. (a) Simulated vertical current flow through the graphene-metal interface for $R_{metal} = R_{graphene}$. The current distribution is radial (b) Simulated current flow through the interface as described in Fig 1(b), i.e., for $R_{metal} \ll R_{graphene}$. The current flow can be described by a one-dimensional model. (c) Optical image of the contact resistance test structure. The structure can be used both for transfer length method measurements to determine the contact resistance and for direct measurements of the specific contact resistivity.

Current density is non-uniformly distributed across the contact area, due to the voltage drop in the graphene. The voltage is highest at the contact edge and drops exponentially with distance. The "1/e" distance of the voltage curve from the front end (x = 0) of the contact is defined as the transfer length L_T (eq. (1)) [3] [9]. In simple terms, transfer length is an effective electrical length of the contact. The metal-graphene contact can be either a line contact or an areal contact depending on the L_T value. The ideal situation would be in the case when L~L_T, which means that almost the entire contact area is responsible for current transmission (areal contact). The term "front contact resistance" is in this context defined as the ratio of the voltage drop across the interfacial layer at that edge of the contact where the current density is greatest to the total current I flowing through the contact. Similarly, end contact resistance is defined as the ratio of the voltage drop across the interfacial layer at the edge of the contact where the current density is least to the total current I flowing through the contact.

Various measurement techniques have been established to measure interfacial contact resistance (ρ_C), sheet resistance under the metal contact (R_{SK}) and sheet resistance of the graphene channel (R_{SH}) between source-drain contact regions [10]–[15]. The method proposed in this work enables the measurement of all relevant values (ρ_C, R_{SH}, R_C) using just one contact test structure [13], [23], [24]. In principle, the test structure consists of line contacts with two contact pads and a variation of the distance between the contacts. The layout is derived from the standard transfer length method proposed by Shockley [17]. The structure requires just two contacts and allows measuring ρ_C directly. The first step is the measurement of R_C by TLM or 4-point/2-point measurements. In a second step, ρ_C is directly measured using the

contact end resistance measurement, which is similar to the CBKR method [26], [27]. In the contact end resistance version in Fig. 1(b), the semiconductor/graphene and the metal lines are crossed and the current is forced to flow around the corner. The CBKR method (generally) consists of forcing a known current through the pads marked with I_{in} and I_{out} [Fig. 1(a)]. Voltage is measured between the pads marked with V_1 and V_2, which are positioned orthogonally to the direction of the current flow. Dividing the voltage difference $V_2 – V_1$ by the forced electric current I yields the interfacial resistance $R_{Interface}$. All contact related values can then be extracted by the equation system after measuring the contact resistance R_C and the interfacial resistance $R_{Interface}$. (eq. (1) and eq. (2), the mathematical derivation is included in the supplementary information).

$$R_C = \sqrt{\rho_C R_{sk}} \tag{1}$$

$$R_{interface} = \frac{\sqrt{\rho_C R_{sk}}}{W} \frac{1}{\sinh \frac{L}{\sqrt{\frac{\rho_C}{R_{sk}}}}} \tag{2}$$

In the proposed contact end resistance design, in analogy to the conventional CBKR method, two contacts are used to measure V_1 and V_2. The advantage of this design is the self-aligning character of this structure, where the channel and the contact just have to cross each other perpendicularly. A simple estimation demonstrates this advantage: if we assume the width of the channel and the metallization to be 1 µm, and further the misalignment to be 1 µm in x and y directions, the conventional CBKR structure will not work. The structure proposed in this work [Fig. 1(b)] would still work without error. The resistor network corresponding to the schematic of the proposed structure is shown in [Fig. 1(c)]. Here, the situation is changed from a 2D problem to a 3D problem. The interface resistance $R_{Interface}$ can be split into
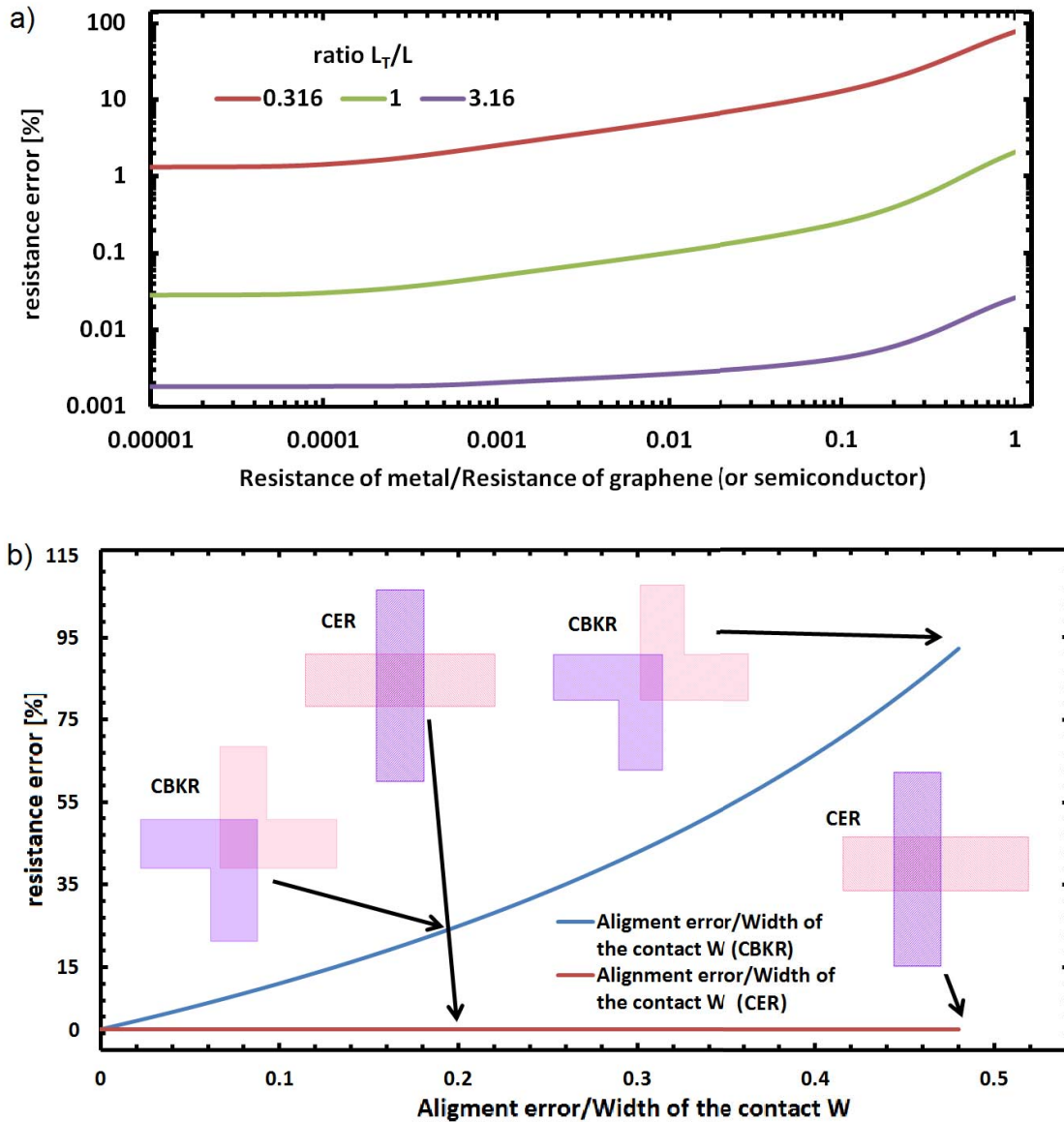
FIGURE 3. (a) The error of the specific contact resistance measurement depends on the metal sheet resistance and the transfer length. In general it should be noted that the error can be manipulated by the experiment/experimenter. By choosing a small L the ratio L_T/L gets larger and a lager ratio leads to a smaller error. As L is the contact length this parameter can be manipulated by the mask set. (b) The error in the resistance depends strongly on the alignment error for the CBKR structure. Whereas the contact end resistance measurement (CER) is not affected by alignment errors.

infinitely small resistors R_{ij}. In the case of negligible metal resistance [Fig. 1(d)] the situation can be simplified because of the symmetry in x-direction. In the case of graphene, neglecting the metal resistance R_M is a valid assumption as the sheet resistance of graphene is much higher than that of the metal, i.e., $R_{sh} \gg R_M$. Thus, all R_{ij} can be combined in the y dimension:

$$\sum_{j=0}^{N} R_{ij} = R_i \qquad (3)$$

The situation is now nearly identical to the conventional CBKR method and ρ_C can be measured with the help of the set of equations discussed above. We evaluated

this hypothesis with simulations using the LTspice V code. First, the resistor network in [Fig. 1(c)] was implemented in LTspice and the resistor values were varied to investigate the current flow path. The results of the simulations for two cases ($R_M = R_{sh}$ and $R_M \ll R_{sh}$) are shown in [Fig. 2(a) and (b)]. The electric current is evaluated directly at the interface, representing only the part in z-direction, i.e., the orange components in Fig. 1. If the metal resistance is in the range of the graphene sheet resistance, the current flow path has a circular/round/edge shape [Fig. 2(a)]. In this case, the current density maximum is located at the edge where the current has to pass through fewer resistors. The situation changes for metal resistances much lower than the graphene

resistance (Fig. 2(b), where the situation becomes symmetric and equations 1 to 2 can be used. In Figs. 3(a) and 3(b), the calculated error trends for this structure are shown. Metal is considered as a perfect conductor due to high charge carrier concentration (10^{22} cm^{-3}). Graphene is a semi metal due to the lack of a band gap and the charge carrier concentration lies in the range of ($10^{10} \sim 10^{12}$ cm^{-2}). Therefore the assumption of neglecting the metal resistance is valid.

III. EXPERIMENT

The proposed method was demonstrated by applying it to Al-graphene contacts, as shown in the optical micrograph in [Fig. 2(c)]. We would like to stress again, that it is favorable for experiments on graphene and other two-dimensional material flakes, as it can be applied to just one contact pair, whereas TLM and CBKR would require two flakes to measure ρ_C and R_{SK}, adding to the variability of experiments. We chose aluminum as the contact metal because it is CMOS compatible and also because the formation of a parasitic interfacial aluminum oxide (Al$_2$O$_3$) can be controlled through process conditions, i.e., the presence of oxygen and/or water.

The devices were fabricated on 280 nm SiO$_2$-coated Si wafers. Single-layer graphene flakes were exfoliated from pure pyrolytic graphite by the adhesive tape method [28]. Two outer metal contacts per device were defined by electron beam (e-beam) lithography and chrome/gold (15/65 nm) thermal evaporation and lift-off. Subsequently, graphene channels (1 μm wide and 10 μm long) were defined in a second e-beam step and structured using oxygen (O$_2$) reactive ion etching, followed by solvent resist stripping with acetone. The areas for the Al contacts were defined afterwards, again by e-beam lithography. 80 nm thick aluminum contacts were deposited by thermal evaporation. One sample ("wet") was dipped into deionized (DI) water for 5 minutes, and aluminum (Al) was then thermally evaporated at a pressure of $\sim 3 \cdot 10^{-5}$ mbar (pumping time ~ 25 min). The other sample ("dry") was not exposed to a DI-water dip, but instead kept in vacuum in the deposition chamber for 24 hours and heated in vacuum at 100°C for 10 min immediately before thermal evaporation of Al at a pressure of $\sim 4 \cdot 10^{-6}$ mbar. The metal deposition was performed in a Tectra Mini-Coater thermal/e-beam evaporation tool. The first procedure is expected to result in a significantly higher amount of adsorbed water at the SiO$_2$ / graphene / metal interfaces. During deposition, aluminum comes into contact with these adsorbed water molecules and is expected to form Al$_2$O$_3$, which increases the ρ_C, similar to such layers in Al/Si interfaces [4], [5]. The details of the fabrication process are shown schematically in Fig. 4.

It should be noted that there might also be other adsorbed chemicals that can influence the graphene, e.g., airborne volatile organic compounds (VOCs). A longer pumping time reduces also the level of these adsorbed molecules.

The presence of an interfacial oxide was experimentally investigated by AES. Since the interpretation of AES results
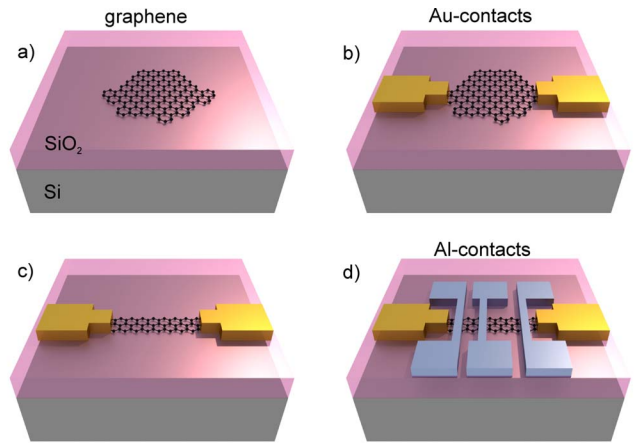
FIGURE 4. Schematic of the fabrication process. (a) Exfoliated graphene is transferred onto 280nm SiO$_2$. (b) Source-drain contacts were defined by e-beam lithography and Stack of Chrome/Gold (15nm/65nm) was deposited by evaporation tool followed by a lift-off process. (c) The graphene channel is patterned using oxygen plasma RIE (Reactive Ion Etching) tool. d) In the final step e-beam lithography was carried out in order to define source-drain contact pads and subsequently aluminum (Al) was deposited.

is difficult on monoatomic graphene layers, specific samples were prepared on thicker graphene (graphite) flakes by the wet and the dry deposition method. While this enables improved imaging in the AES, the surface chemistry behavior can be assumed identical to graphene. AES spectra were recorded on a PHI 700 spectrometer using 10 kV primary electron energy and 10 nA electron current with charge compensation by low-energy Ar$^+$ ions. Depth profiling was done with 500 eV Ar$^+$ ions resulting in a sputter rate of 8 nm/min SiO$_2$ equivalent [Fig. 5(a) and Fig. 5(b)]. The large chemical shift in the Auger electron spectrum between Al and Al$_2$O$_3$ allows to clearly differentiate between the two materials. Increased Al$_2$O$_3$ and O concentrations at the sample surface, originating from the native oxide on aluminum, reveal significantly increased oxide formation at the Al/graphene interface of the non-annealed "wet" sample [Fig. 5(a)] compared to the "dry" sample [Fig. 5(b)]

Both types of graphene/aluminum contacts were electrically analyzed according to the proposed method with an EG&G 7260 DSP Lock-in Amplifier at ambient conditions. The I-V curves were linear in the measured region. All measurements were taken at the charge neutrality point (CNP). The interface resistance R$_{Interface}$ in the case of the "wet" sample is 95 kΩ, whereas the "dry" sample shows a value of 7 kΩ. We attribute the significant increase in the contact resistance to the Al$_2$O$_3$ formation at the graphene-metal interface in the "wet" sample, as indicated by AES data. The TLM measurements of the R$_C$ were only conclusive for the "dry" sample. The values for the "wet" sample vary too much for a meaningful interpretation due to Al$_2$O$_3$ formation. An R$_C$ value of 22 ± 0.2 kΩ was found for the dry sample.
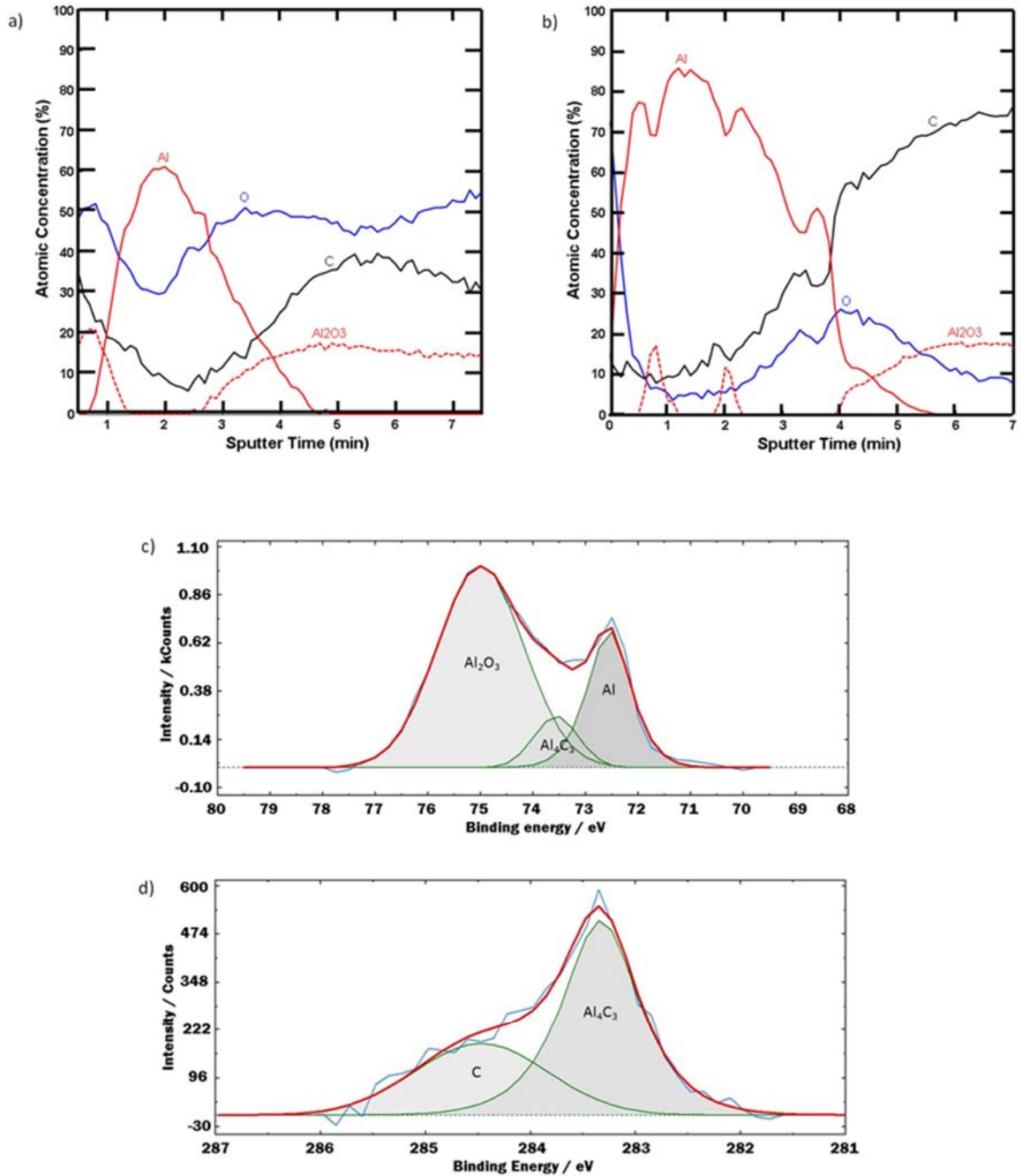
FIGURE 5. (a) Auger depth profile through an Al coated graphite sample under "wet" conditions. At the Al/graphite interface (sputter-time of 3 min) the oxygen concentration increases. Furthermore, Al_2O_3 formation is indicated by the peak shift of the Al signal at the interface to the graphite. The Al_2O_3 at the top surface indicates the native oxide. (c) and (d) XPS spectra taken at the Al/C interface of a "dry" sample. (c) The Al2p signal reveals three species Al, Al_2O_3 and Al_4C_3 (d) The C1s signal supports the existence of Al_4C_3.

The extraction value of L_T is 0.3 μm. This value indicates that the conventional simplification of assuming $L \gg L_T$ is not valid. Therefore, (1) has to be modified with the length dependency:

$$R_C = \frac{\sqrt{R_{SK}\rho_C}}{Z} \coth \frac{L}{L_T} \qquad (4)$$

In order to calculate the sheet resistance under the metal contact (R_{SK}), the value of ρ_C, R_C and L_{TK} were calculated

with the equation shown above. From (4) and (2), an R_{SK} of 38 kΩ/$\square$ has been extracted, which is dramatically higher than the graphene channel resistance of 1150 Ω/$\square$. A value of $1.1 \cdot 10^{-4}$ Ωcm^2 was found for ρ_C. A schematic of the different measurement configurations is shown in the supplementary information (Fig. S2).

To make sure that this high graphene sheet resistance under the contact is not just an error introduced by the measurement method, XPS was carried out to understand

the chemical nature of the graphene-metal junction. In particular, the stacks were investigated with regards to aluminum carbide formation (Al_4C_3). We again used a thicker graphite flake to investigate a "dry" sample in an ULVAC-PHI VersaProbe II using monochromatized Al-K_α radiation and an analyzer pass energy of 29 eV. Charge compensation was achieved by simultaneous electron and low-energy Ar^+ ion irradiation. Sputter depth profiling was done using 250 eV Ar^+ ions. After each sputter cycle, detail spectra were recorded. After completing the depth profile, the Al2p and C1s spectra recorded directly from the interface between Al and graphite were analyzed [Fig. 5(e) and (f)]. The presence of three compounds at the interface between aluminum and graphene can clearly be identified. Their XPS peaks can be assigned to metallic Aluminum, aluminum oxide and aluminum carbide. The chemical shifts of both the Al2p and C1s signals correspond quite well with literature data, which report binding energies of 282.2 eV for C1s in Al_4C_3 and 73.4 eV for Al 2p in Al_4C_3, 72.6 eV for Al 2p in metallic Al, 74.6 eV for Al 2p in Al_2O_3, and 284.5 eV for C 1s in graphitic carbon. Thus, XPS measurements clearly support the model of a carbide formation at the graphene-aluminum interface. The carbide formation leads to chemical bonding between the graphene and the metal and reduces the charge carrier density. This explains the increase of the graphene sheet resistance under the metal, as extracted by the proposed method. Results from other groups on graphene with 30 to 100 nm thick Al top gate structures showed the formation of a few nm thick Al_2O_3 interface layer between graphene and aluminum after exposure to air due to oxygen diffusion into the structure. However, in these experiments no additional water desorption steps prior to Al deposition were reported [29], [30]. In this work, in the case of the "dry" sample, adsorbed water was mostly removed by extended pumping and heating prior to the aluminum deposition allowing the formation of Al_4C_3 in an oxygen-deficient environment. In contrast, in an oxygen-rich environment the formation of Al_2O_3 is thermodynamically favored (enthalpy of formation: -209 kJ/mol for Al_4C_3 and -1676 kJ/mol for Al_2O_3). Once Al_4C_3 is formed at the contact interface, the subsequent formation of a passivating Al_2O_3 layer is kinetically hindered. In addition, the lower density of adsorbed water molecules serving as nucleation sites for aluminum deposition could lead to a lower grain boundary density thus reducing oxygen diffusion through the aluminum film.

IV. CONCLUSION

We demonstrated measurements of the specific contact resistivity (ρ_C) of graphene-metal contacts. This method is derived from a TLM and contact end resistance measurement, utilizing simplified "crossed" contacts instead of rectangular contacts (CBKR). One of the advantages of this method is that it allows the use of small contacts, because the test structure has a self-aligning character. Furthermore it is possible to measure all relevant contact parameters in one contact pair. Two different samples were analyzed,

a "wet" sample with a high amount of Al_2O_3 at the interface and a "dry" one where carbide formation occurred. A significant difference in $R_{Interface}$ was found between the two samples. In the "dry" sample we measured a $R_{Interface}$ of 7kΩ. The "wet" sample in contrast shows a $R_{Interface}$ value of 95 kΩ. The specific contact resistivity extracted was $\rho_C = 1.1 \cdot 10^{-4}$ Ωcm^2. In the "dry" sample, AES and XPS analyses revealed interfacial aluminum carbide that strongly increased R_{SK}. Splitting R_C in ρ_C and R_{SK} the method is highly suitable for investigating electrical contacts to the growing range of two-dimensional materials. This work should serve to investigate and understand the large differences for graphene (and 2D material) - metal contacts using the same contact material.

REFERENCES

[1] Y. Taur and T. H. Ning, *Fundamentals of Modern VLSI Devices*. Cambridge, U.K.: Cambridge Univ. Press, 2013.

[2] C. Y. Chang, Y. K. Fang, and S. M. Sze, "Specific contact resistance of metal–semiconductor barriers," *Solid-State Electron.*, vol. 14, no. 7, pp. 541–550, 1971.

[3] M. Hajłasz *et al.*, "Sheet resistance under Ohmic contacts to AlGaN/GaN heterostructures," *Appl. Phys. Lett.*, vol. 104, no. 24, Jun. 2014, Art. no. 242109.

[4] A. Y. C. Yu, "Electron tunneling and contact resistance of metal–silicon contact barriers," *Solid-State Electron.*, vol. 13, no. 2, pp. 239–247, Feb. 1970.

[5] H. M. Naguib and L. H. Hobbs, "AL/Si and Al/Poly-Si contact resistance in integrated circuits," *J. Electrochem. Soc.*, vol. 124, no. 4, pp. 573–577, 1977.

[6] K. Nagashio, T. Nishimura, K. Kita, and A. Toriumi, "Contact resistivity and current flow path at metal/graphene contact," *Appl. Phys. Lett.*, vol. 97, no. 14, 2010, Art. no. 143514.

[7] J. T. Smith, A. D. Franklin, D. B. Farmer, and C. D. Dimitrakopoulos, "Reducing contact resistance in graphene devices through contact area patterning," *ACS Nano*, vol. 7, no. 4, pp. 3661–3667, Apr. 2013.

[8] W. S. Leong, H. Gong, and J. T. L. Thong, "Low-contact-resistance graphene devices with nickel-etched-graphene contacts," *ACS Nano*, vol. 8, no. 1, pp. 994–1001, Jan. 2014.

[9] V. Passi *et al.*, "Contact resistance study of 'edge-contacted' metal–graphene interfaces," presented at the ESSDERC, Lausanne, Switzerland, 2016.

[10] M. Shaygan *et al.*, "Low resistive edge contacts to CVD-grown graphene using a CMOS compatible metal," *Annalen der Physik*, vol. 529, no. 11, Nov. 2017, Art. no. 1600410.

[11] L. Anzi *et al.*, "Ultra-low contact resistance in graphene devices at the dirac point," *2D Mater.*, vol. 5, no. 2, 2018, Art. no. 025014.

[12] K. Nagashio and A. Toriumi, "Density-of-states limited contact resistance in graphene field-effect transistors," *Jpn. J. Appl. Phys.*, vol. 50, no. 7, p. 0108, 2011.

[13] H. Y. Park *et al.*, "Extremely low contact resistance on graphene through n-type doping and edge contact design," *Adv. Mater.*, vol. 28, no. 5, pp. 864–870, 2016.

[14] F. Xia, V. Perebeinos, Y.-M. Lin, Y. Wu, and P. Avouris, "The origins and limits of metal–graphene junction resistance," *Nat. Nanotechnol.*, vol. 6, no. 3, pp. 179–184, Mar. 2011.

[15] H. Xu *et al.*, "Properties of graphene–metal contacts probed by Raman spectroscopy," *Carbon*, vol. 127, pp. 491–497, Feb. 2018.

[16] D. K. Schroder, *Semiconductor Material and Device Characterization*. New York, NY, USA: Wiley, 2006.

[17] M. Ono, A. Nishiyama, and A. Toriumi, "A simple approach to understanding measurement errors in the cross-bridge Kelvin resistor and a new pattern for measurements of specific contact resistivity," *Solid-State Electron.*, vol. 46, no. 9, pp. 1325–1331, Sep. 2002.

[18] S. Wang *et al.*, "Characterization of the quality of metal–graphene contact with contact end resistance measurement," *Appl. Phys. A, Solids Surf.*, vol. 122, no. 7, p. 643, Jul. 2016.

[19] N. Stavitski, J. H. Klootwijk, H. W. van Zeijl, A. Y. Kovalgin, and R. A. M. Wolters, "Cross-bridge Kelvin resistor structures for reliable measurement of low contact resistances and contact interface characterization," *IEEE Trans. Semicond. Manuf.*, vol. 22, no. 1, pp. 146–152, Feb. 2009.

[20] S. Wang *et al.*, "A more reliable measurement method for metal/graphene contact resistance," *Nanotechnology*, vol. 26, no. 40, Oct. 2015, Art. no. 405706.

[21] S.-A. Peng *et al.*, "The sheet resistance of graphene under contact and its effect on the derived specific contact resistivity," *Carbon*, vol. 82, pp. 500–505, Feb. 2015.

[22] S. Dimitrijev, *Principles of Semiconductor Devices*. New York, NY, USA: Oxford Univ. Press, 2012.

[23] A. Gahoi *et al.*, "Contact resistance study of various metal electrodes with CVD graphene," *Solid-State Electron.*, vol. 125, pp. 234–239, Nov. 2016.

[24] J. S. Moon *et al.*, "Ultra-low resistance ohmic contacts in graphene field effect transistors," *Appl. Phys. Lett.*, vol. 100, no. 20, May 2012, Art. no. 203512.

[25] W. Shockley, "Research and investigation of inverse epitaxial UHF power transistors," Air Force At. Lab., Wright–Patterson Air Force Base Ohio, Dayton, OH, USA, Rep. Al-TOR-64-207, 1964.

[26] S. J. Proctor, L. W. Linholm, and J. A. Mazer, "Direct measurements of interfacial contact resistance, end contact resistance, and interfacial contact layer uniformity," *IEEE Trans. Electron Devices*, vol. 30, no. 11, pp. 1535–1542, Nov. 1983.

[27] S. J. Proctor and L. W. Linholm, "A direct measurement of interfacial contact resistance," *IEEE Electron Device Lett.*, vol. 3, no. 10, pp. 294–296, Oct. 1982.

[28] K. S. Novoselov *et al.*, "Electric field effect in atomically thin carbon films," *Science*, vol. 306, no. 5696, pp. 666–669, 2004.

[29] S.-L. Li, H. Miyazaki, A. Kumatani, A. Kanda, and K. Tsukagoshi, "Low operating bias and matched input-output characteristics in graphene logic inverters," *Nano Lett.*, vol. 10, no. 7, pp. 2357–2362, Jul. 2010.

[30] E. Guerriero *et al.*, "Graphene audio voltage amplifier," *Small*, vol. 8, no. 3, pp. 357–361, 2012.

AMIT GAHOI received the M.Sc. degree in nanotechnology from the KTH Royal Institute of Technology, Stockholm, Sweden, in 2013. He is currently pursuing the Ph.D. degree in electrical contacts to 2-D materials with RWTH Aachen University, Aachen, Germany. His current research areas include semiconductor test structures and microfabrication/nanofabrication technologies.

SEBASTIAN WITTMANN received the M.Sc. degree in applied research in engineering sciences from OTH Regensburg, Germany. He is currently pursuing the Ph.D. degree with Infineon Technologies AG, Regensburg, and RWTH Aachen University. His current research interests include nanoelectronic devices and sensors made from novel 2-D materials like graphene and their integration into CMOS compatible device environments.

TOBIAS PREIS received the M.Sc. degree in physics from the University of Regensburg, Regensburg, Germany, where he is currently pursuing the Ph.D. degree. His current research interest is focused on chemically derived graphene nanoribbons and their electronic characterization.

JOERG-MARTIN BATKE was born in 1973. He received the Dipl.-Phys. and Dr.rer.nat. degrees in solid state physics from Regensburg University, Regensburg, Germany, in 1999 and 2003, respectively. He is currently a Surface Analytical Expert with Infineon Technologies, leading the company-wide user group on this field with a focus of attention on coordinating knowledge exchange, consulting, and mentoring.

IOAN COSTINA, photograph and biography not available at the time of publication.

MATTHIAS KÖNIG received the Master of Science degree in physics from the University of Regensburg, Regensburg, Germany. He is currently pursuing the Ph.D. degree with RWTH Aachen University. He is a Development Engineer with TDK Electronics AG. His current research interests include nanoelectromechanical devices and sensors and their integration into the silicon technology platform.

GÜNTHER RUHL received the Diploma and Doctoral degrees in chemistry from the Technical University of Munich, Germany. After working with Infineon Technologies as a Lead Principal for New Materials, he is currently a Research Fellow with the Deggendorf Institute of Technology, Germany. His current research interests include sensors made from novel materials like graphene and related 2-D materials and their integration into silicon and glass technology platforms.

MAX C. LEMME (M'00–SM'06) received the Dipl.-Ing. and Dr.-Ing. degrees in electrical engineering from RWTH Aachen University, Aachen, Germany, where he is currently a Professor of electronic devices. He is also the Director of AMO GmbH, Aachen. His current research interests include electronic, optoelectronic and nanoelectromechanical devices and sensors made from novel materials like graphene and related 2-D materials, perovskites or phase change materials and their integration into the silicon technology platform.